Neurotherapeutics
DOI 10.1007/s13311-013-0255-9

ORIGINAL ARTICLE

Chronic Treatment with 17-DMAG Improves Balance and Coordination in A New Mouse Model of Machado-Joseph Disease

Anabela Silva-Fernandes · Sara Duarte-Silva · Andreia Neves-Carvalho · Marina Amorim · Carina Soares-Cunha · Pedro Oliveira · Kenneth Thirstrup · Andreia Teixeira-Castro · Patrícia Maciel

Abstract Machado-Joseph disease (MJD) or spinocerebellar ataxia type 3 (SCA3) is a neurodegenerative disease currently with no treatment. We describe a novel mouse model of MJD which expresses mutant human ataxin-3 at near endogenous levels and manifests MJD-like motor symptoms that appear gradually and progress over time. CMVMJD135 mice show ataxin-3 intranuclear inclusions in the CNS and neurodegenerative changes in key disease regions, such as the pontine and dentate nuclei. Hsp90 inhibition has shown promising outcomes in some neurodegenerative diseases, but nothing is known about its effects in MJD. Chronic treatment of CMVMJD mice with Hsp90 inhibitor 17-DMAG resulted in a delay in the progression of their motor coordination deficits and, at 22 and 24 weeks of age, was able to rescue the uncoordination phenotype to wild-type levels; in parallel, a reduction in neuropathology was observed in treated animals. We observed limited induction of heat-shock proteins with treatment, but found evidence that 17-DMAG may be acting through autophagy, as LC3-II (both at mRNA and protein levels) and beclin-1 were induced in the brain of treated animals. This resulted in decreased levels of the mutant ataxin-3 and reduced intranuclear aggregation of this protein. Our data validate this novel mouse model as a relevant tool for the study of MJD pathogenesis and for pre-clinical studies, and show that Hsp90 inhibition is a promising therapeutic strategy for MJD.

Keywords Polyglutamine · animal models · ataxia · behavior · therapy · autophagy.

Anabela Silva-Fernandes and Sara Duarte-Silva contributed equally to this work

Electronic supplementary material The online version of this article (doi:10.1007/s13311-013-0255-9) contains supplementary material, which is available to authorized users.

A. Silva-Fernandes · S. Duarte-Silva · A. Neves-Carvalho · M. Amorim · C. Soares-Cunha · A. Teixeira-Castro · P. Maciel (✉)
Life and Health Sciences Research Institute (ICVS), School of Health Sciences, University of Minho, Braga, Portugal
e-mail: pmaciel@ecsaude.uminho.pt

A. Silva-Fernandes · S. Duarte-Silva · A. Neves-Carvalho · M. Amorim · C. Soares-Cunha · A. Teixeira-Castro · P. Maciel
ICVS/3B's - PT Government Associate Laboratory, Braga/Guimarães, Portugal

P. Oliveira
ICBAS - Abel Salazar Biomedical Sciences Institute, University of Porto, Porto, Portugal

K. Thirstrup
Dept. of Neurodegeneration, H. Lundbeck A/S, Valby, Denmark

Introduction

Machado-Joseph disease (MJD), also known as spinocerebellar ataxia type 3 (SCA3), is caused by a CAG repeat expansion (>55) [1] in the protein coding region of the *ATXN3* gene, located in chromosome 14q32.1 and encoding the protein ataxin-3. The main clinical features of MJD are ataxia and ophthalmoplegia, which can be associated to a variable degree with peripheral amyotrophy, intention fasciculation-like movements of facial and lingual muscles, rigidity, spasticity, dystonia and palpebral retraction, leading to the appearance of bulging eyes [2]. Ataxin-3 harboring the expanded polyQ tract has a strong tendency for aggregation, leading to the formation of inclusions in the nucleus and cytoplasm of neuronal cells, including axonal tracts [3, 4], the pathogenic relevance of which remains unclear.

Molecular chaperones are crucial for the maintenance of native protein conformation, and recent research has shown that defective chaperone action may have pathogenic consequences [5, 6]. Several studies demonstrated the involvement of the heat shock proteins in MJD [7–10]; co-localization of Hsp70, Hsp40 and Hsp90, but not other chaperones (Hsp27, Hsp60 and Hsp110) with aggregates formed by mutant ataxin-3 has been described, which might result in a depletion of these protective molecules [7, 9]. In order to promote the correct refolding of the pathogenic protein(s) and to reduce the formation of toxic aggregated forms, the use of compounds that promote increased expression of heat shock proteins (HSPs), leading to improved protein folding and/or clearance of the mutant protein by the ubiquitin proteasome system or through autophagy, has been proposed [11, 12]. Hsp90, by itself and/or associated with multichaperone complexes, is a major repressor of HSF-1 acting in a feedback regulation mechanism [13]. Pharmacologic inactivation of Hsp90 leads to the overexpression of several molecular chaperones, activating the heat-shock response (HSR) *via* the persistence of HSF-1 action [13, 14]. Potent Hsp90 inhibitors, such as 17-AAG or 17-DMAG, have been shown to reduce aggregate load and toxicity in cell, fly, nematode and mouse models of several neurodegenerative diseases, dependently on HSF-1 [15–20]. Concerning polyQ diseases, these two compounds have been shown to have beneficial effects only for SBMA [19–21]. Despite its high potency, 17-AAG showed poor solubility and stability and demonstrated moderate toxicity in several clinical trials [22]. In contrast, 17-DMAG is a more potent analog of 17-AAG [23], is more water soluble than 17-AAG and can be administered orally [24], which could be advantageous for clinical purposes.

Although mouse models have been a remarkable tool in human disease research, several criteria have to be achieved in order to validate a genetically manipulated mouse as a model of a disease [25]. Therapeutic trials need to be performed in animal models showing significant similarities to the human diseases, in order to better evaluate the therapeutic benefit of a specific compound. Although several transgenic mouse models have been generated for the study of MJD, it has been difficult to find in one single model the main features of this disorder (reviewed in [26]).

In this work, we generated a new transgenic mouse model expressing ATXN3 with 135 glutamines under the control of the CMV promoter. These mice develop a progressive neurological disease overlapping with the core clinical features of MJD and show relevant neuropathology as well as ubiquitin-positive ataxin-3 intranuclear inclusions in regions of the brain known to be involved in MJD, including the pontine and deep cerebellar nuclei. We used this model in a pre-clinical trial to validate Hsp90 inhibition as a therapeutic strategy for MJD, with encouraging results that suggest that this approach should be pursued.

Results

CMVMJD135 Mice Express the Expanded Human Ataxin-3 in the CNS

We have generated transgenic mice expressing the ATXN3c cDNA variant of the *ATXN3* gene carrying a repeat tract with the sequence $(CAG)_2CAAAAGCAGCAA(CAG)_{129}$, coding for 135 glutamines, under the regulation of the CMV promoter (Fig. 1A). Transgene mRNA quantification demonstrated that one lineage (hereafter designated CMVMJD135), expressed the human ATXN3 protein in the brain (Fig. 1B). This lineage, possessing two copies of the transgene, expressed the human *ATXN3* mRNA at near-endogenous levels in the cerebellum, brainstem, forebrain and spinal cord (Fig. 1C). When breeding these animals we observed intergenerational CAG repeat length variation, mostly towards contraction (Supplementary Fig. 1) (maternal meioses (n=24): mean=−1.46±2.74; range=[−7, +4]; paternal meioses (n=42): mean=−0,71±1,61; range=[−5, +1]). We chose to study animals with repeat lengths over 129. All the comparisons for the genotype factor were performed between CMVMJD135 mice and wild-type littermates since it has been previously shown that transgenic mice expressing human ataxin-3 carrying a normal CAG repeat tract did not display any differences in the phenotype or neuropathology in comparison with wild-type (wt) [27–30]. In addition, our previous data have shown that even expression of ataxin-3 with 83 glutamines under the CMV promoter caused no phenotype change [31].

CMVMJD135 Transgenic Mice Display Progressive Neurological Deficits

At 4 weeks of age, transgenic and control littermates were indistinguishable in their home cage; however, at 16 weeks of age transgenic animals started to present a visibly abnormal gait and at 40 weeks of age they showed an unhealthy appearance, an abnormal body posture, limb clasping and limb tonus deficit (Fig. 1D).

Female CMVMJD135 transgenic and control mice gained weight at a similar rate until 19 weeks of age (Fig. 1E); however, transgenic males showed a significantly lower body weight gain compared with control males at 19 weeks of age, and since this age, all transgenic animals demonstrated a decline in body weight, whereas their wt littermates continued to gain weight until 40 weeks of age (male: genotype x age, $F_{2,61}$=35.067, p<0.000; female: genotype x age, $F_{2,61}$=5.211, p=0.008).

In the balance beam test, CMVMJD135 mice showed a significantly worse performance already at 10 weeks of age traversing the medium square beam (male: genotype, $F_{1,40}$= 30.845, $p=2\times10^{-6}$, age, $F_{1,40}$=6.356, p=0.014; female: genotype, $F_{1,44}$=10.754, p=0.002) (Fig. 2B), as well as the medium (male: genotype, $F_{1,34}$=22.023, $p=4.3\times10^{-5}$; female:

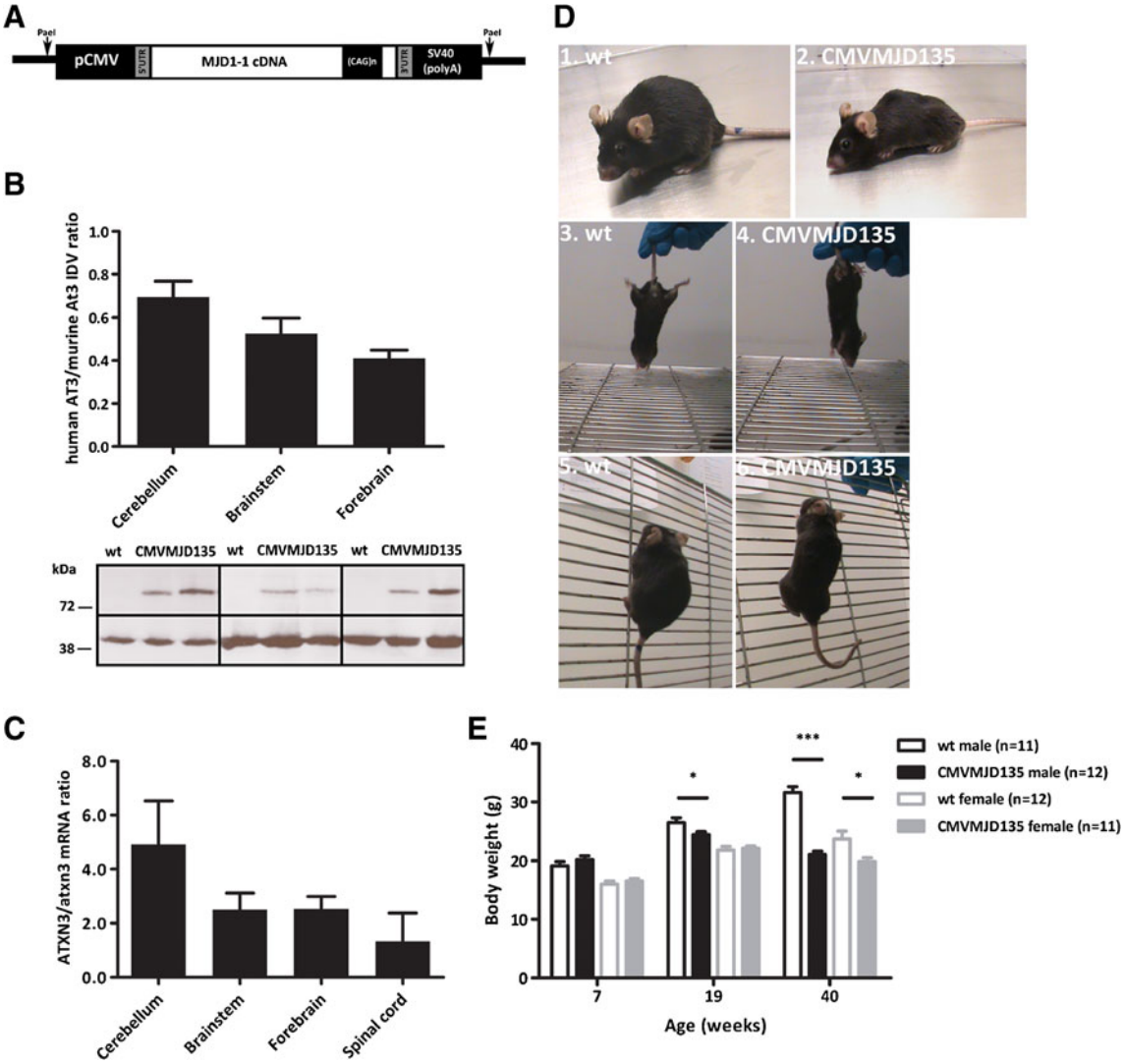

Fig. 1 Generation of a transgenic mouse model of MJD carrying the expanded ATXN3 with 135 CAGs. (A) Schematic diagram of the plasmid CMVMJDAT3Q135_1.5 used for the generation of cDNA MJD transgenic mice. (B) Western blot anti-ATXN3 in different CNS regions (cerebellum, forebrain and brainstem) of CMVMJD135 mice with 14–16 weeks of age. In all lanes, the endogenous mouse ataxin-3 (Atxn3) is detected at about 42 kDa. An approximately 80-kDa protein corresponding to expanded ATXN3 is detected in transgenic animal lysates. (C) qRT-PCR analysis of human ATXN3 and murine Atxn3 mRNA expression levels. Values are presented as mean ± SEM (n=4). (D) CMVMJD135 mice at 40 weeks of age presenting body posture deficit with lower pelvic elevation and hunchback (2), limb clasping (4) and reduced hindlimb tonus (6) in comparison with wt animals (1,3,5). (E) Assessment of body weight with age (n=11–12 for each group). Asterisks indicate significant differences between wt control and CMVMJD135 transgenic mice. *p<0.05, **p<0.01, ***p<0.001

genotype, $F_{1,37}$=4.859, p=0.034) (Fig. 2D) and the small round beams (male: genotype, $F_{1,31}$=18.486, p=1.58×10^{-4}; female: genotype, $F_{1,34}$=11.487, p=0.002, age, $F_{1,34}$=5.618, p=0.024) (Fig. 2E). With disease progression, CMVMJD135 mice demonstrated a higher frequency of foot slips and a flattened body posture in the beams. By 40 weeks of age, transgenic mice failed to maintain balance on the beams and fell off.

Footprint patterns of wt (41 weeks of age) and CMVMJD135 transgenic mice at 14, 28 and 41 weeks of age are illustrated in Fig. 3A. Dragging of the feet was observed in transgenic animals already at 14 weeks of age, progressing through age and becoming increasingly more severe (41 weeks: p=2.44×10^{-4}) (Fig. 3B). Additionally, beginning at 16 weeks of age, transgenic mice displayed a reduced paw overlap when compared with control animals, indicating an altered uniformity of step alternation (genotype, $F_{1,11}$=5.184, p=0.044) (Fig. 3C) as well as a significant decrease in the stride length (genotype, $F_{1,11}$=36.086, p=8.8×10^{-5}) (Fig. 3D).

CMVMJD135 mice swam significantly slower than control littermates at 22–25 weeks of age (genotype, $F_{1,21}$= 17.927, p=3.71×10^{-4}) and more so at 40 weeks (genotype, $F_{1,15}$=42.466, p=1.0×10^{-5}) (Fig. 4A). In addition, they displayed abnormalities in their swimming movements, adopting a twisted posture, and kicked in an uncoordinated

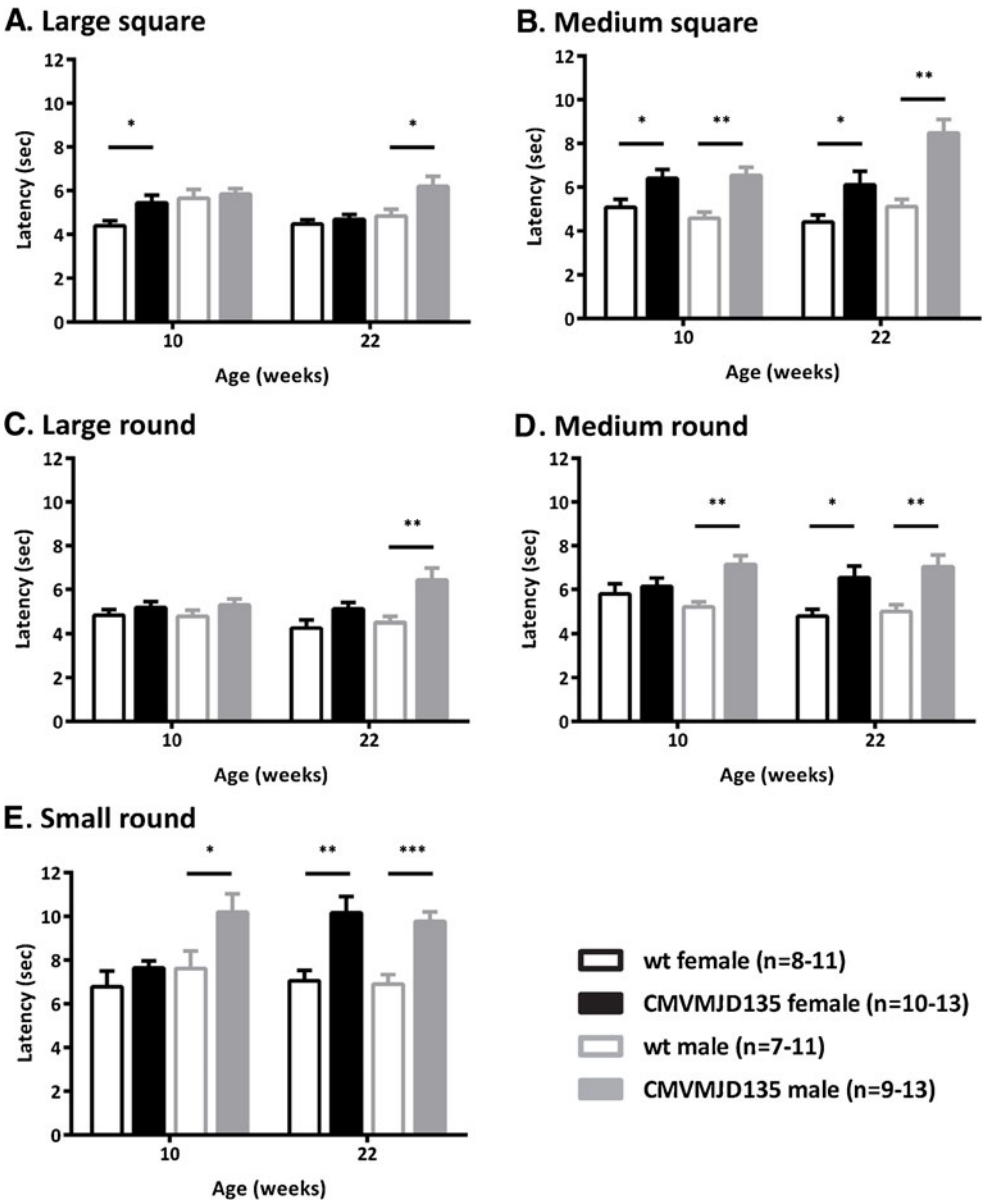

Fig. 2 Body balance impairment in CMVMJD135 mice. Balance beam test performance of wt and transgenic animals using square (A,B) and round beams (C–E) is depicted at 10 and 22 weeks of age. Values are presented as mean ± SEM (n=8–13 for each genotype and gender). *p<0.05, **p<0.01, ***p<0.001

manner with both hind- and forelimbs. In the rotarod paradigm, significant differences were observed from the age of 20 weeks (genotype, $F_{1,21}$=4.879, p=0.038) (Fig. 4B). At 40 weeks of age, transgenic animals showed a dramatic deterioration in their rotarod performance compared with littermate controls, both in the accelerating rod (genotype, $F_{1,17}$=20.234, p=3.17×10^{-4}) and at constant speeds (8 rpm: p=0.004; 15 rpm: p=0.002; 20 rpm: p=0.003; 24 rpm: p=0.002) (Fig. 4C).

At the first age of assessment with the SHIRPA protocol (7 weeks) CMVMJD135 transgenic mice revealed significant differences in performance in the hanging wire grip test, that became worse with age (male: genotype x age, $F_{1,42}$=30.331, p=2.0×10^{-6}; female: genotype x age, $F_{1,41}$=36.955, p<0.000) (Fig. 5A). At 19 weeks of age, a significant percentage of transgenic animals developed loss of hindlimb tonus resistance (male: p=1.07×10^{-4}; female: p=0.002) (Fig. 5B), a decrease in forelimb strength (male: p=0.003; female: p=0.006) (Fig. 5C) and hindlimb clasping (male: p=1.07×10^{-4}; female: p=0.006) (Fig. 5D). Furthermore, 40-week-old animals demonstrated a dramatic deterioration of the neurological symptoms observed at 19 weeks of age in the SHIRPA protocol, namely, the loss of hindlimb tonus, the tremors and the decreased locomotor and exploratory activity, among others (Supplementary Fig. 2A–D). From 40 weeks of age onwards, most CMVMJD135 mice were not able to traverse the beams or stay in the rotarod and their footprinting pattern was difficult to measure due to the severe dragging, which led us to halt the phenotype evaluation.

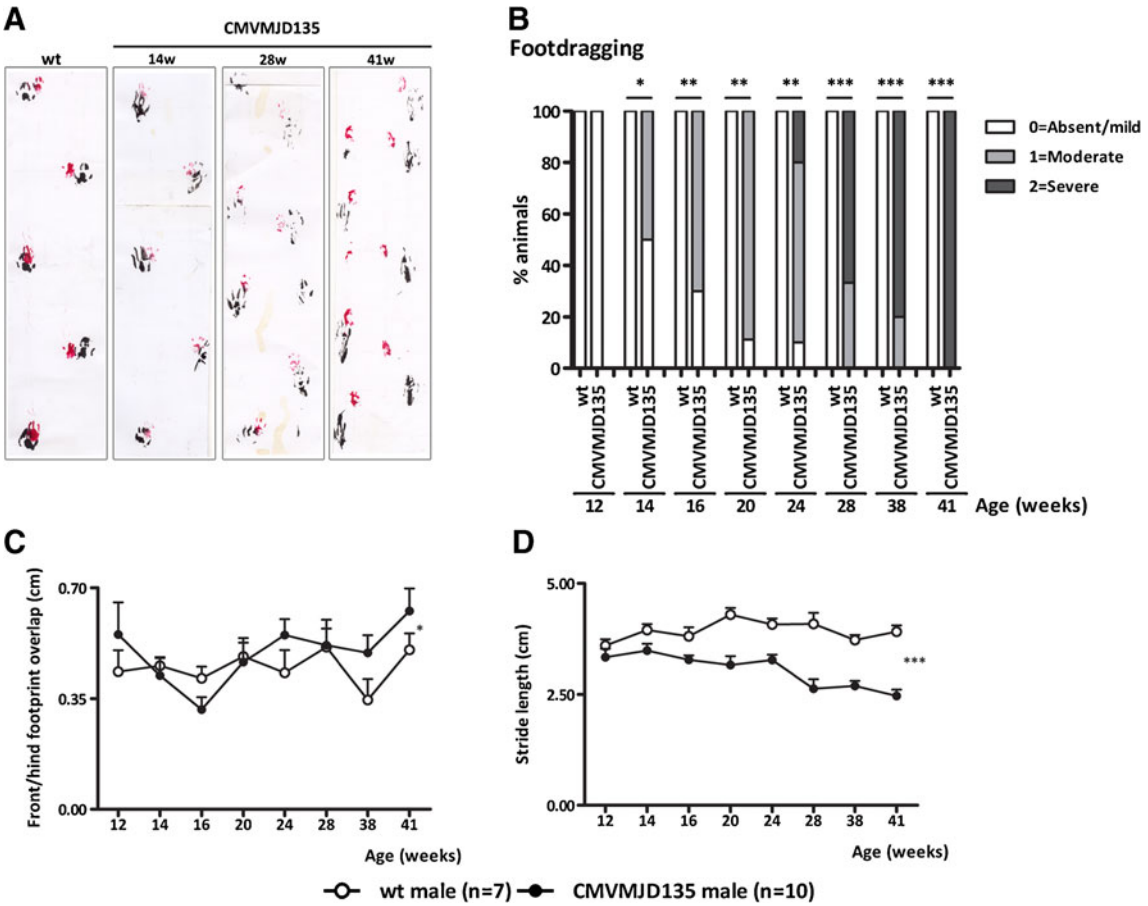

Fig. 3 Abnormal footprint pattern in transgenic mice. (A) Representative walking footprint patterns of 14-, 28- and 41-week-old CMVMJD135 mice. Qualitatively, the patterns generated clearly differ, showing that transgenic mice display foot-dragging. At late stages CMVMJD135 mice also demonstrate shorter strides and an irregular left–right step pattern as compared with the wt control mice. (B) Quantitative analysis of foot-dragging. Quantitative analysis of the footprint patterns of wt and transgenic mice, based on measurements of (C) distance between front and hind footprint overlap and (D) stride length through age. Values are presented as mean ± SEM (n=7 and 10 for wt and transgenic, respectively). *p<0.05, **p<0.01, ***p<0.001

A group of wt (n=9) and transgenic animals (n=13) were followed through life until they had to be sacrificed due to established humane endpoints (93 weeks of age). Although transgenic mice showed a progressive deterioration of the motor phenotype, no differences were observed in survival rate between both genotypes until this age, in the laboratory conditions used, which included lowering the food to an accessible level and hydrating it at ages when transgenic animals had difficulty reaching the food and drink compartments.

For cognitive assessment, the Morris Water Maze test was performed at 10 weeks of age, before the motor symptoms would interfere excessively with testing, and no differences were found (Supplementary Fig. 2E,F).

CMVMJD135 Mice Exhibit Reduced Brain Weight, Reduced Volume and Total Cell Number in Pontine Nuclei and Intranuclear Ataxin-3 Inclusions

The total brain weight of CMVMJD135 mice was slightly reduced (5 %) in comparison with control littermates at late stages of the disease (42–43 weeks) (p=2.74×10^{-4}) (Fig. 6A). However, we did not observe differences in brain weight in animals sacrificed at 20 weeks of age, suggesting that the motor phenotype begins before marked neuronal loss. Stereological evaluation of CMVMJD135 mice brains at 60 weeks of age revealed a significantly reduced volume as well as a decrease in total cell number in pontine nuclei indicating neuronal demise in this region, known to be affected in MJD (Fig. 6B). Interestingly, transgenic mice showed a significant volume reduction without cell loss in the dentate nuclei. In contrast, no differences were found in the locus coeruleus and in the substantia nigra (SN), although hyperchromatic cells and astrogliosis were observed in SN (Fig. 6C; Supplementary Fig. 3).

Immunohistochemistry showed the presence of ataxin-3 inclusions in the nucleus of neuronal cells in different regions of the CNS of CMVMJD135 mice at 20–35 weeks of age (Fig. 6C) including the pontine nuclei, reticulotegmental nucleus of the pons, spinal cord neurons, the facial nuclei, anterior olfactory nuclei, ventral tenia tecta, inferior olive,

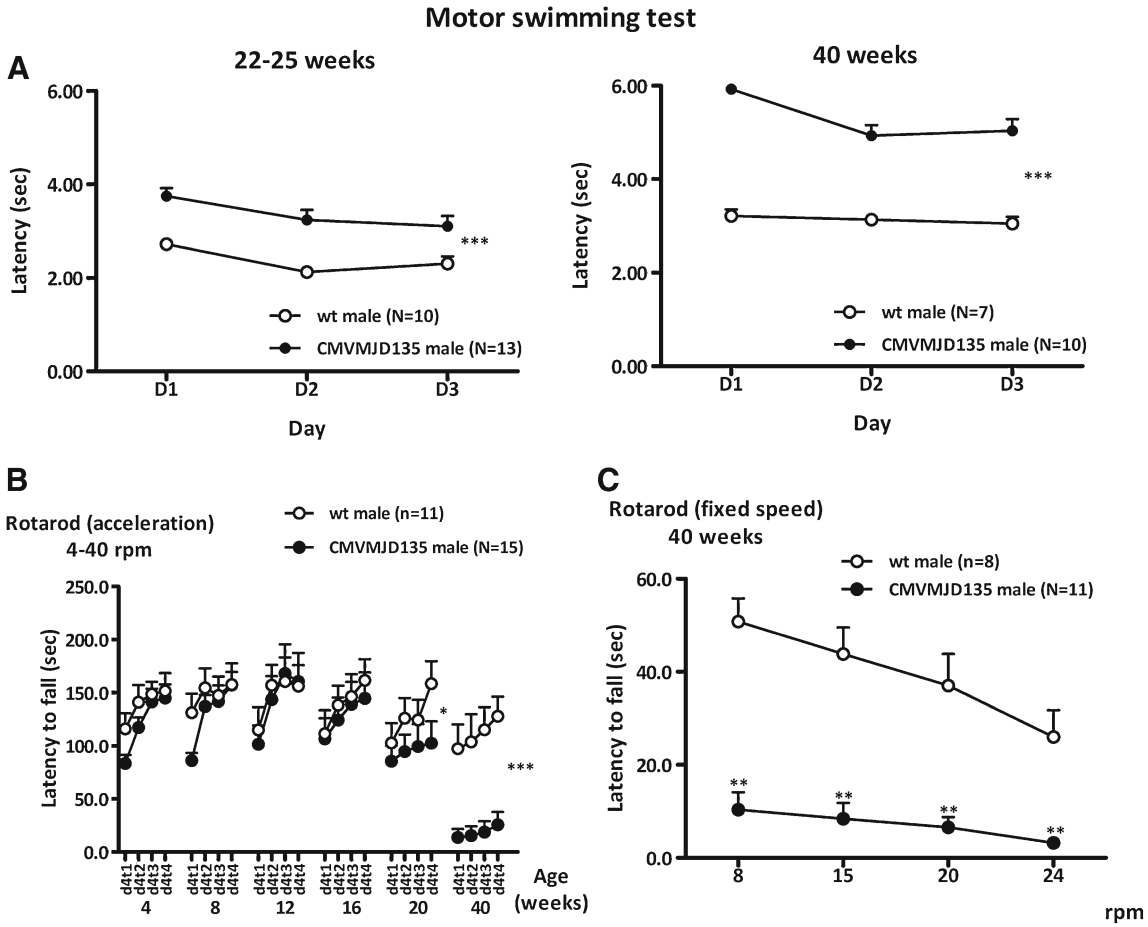

Fig. 4 Motor incoordination on the rotarod and in the swimming tank in CMVMJD135 mice. (A) 22–25- and 40-week-old wt and CMVMJD135 male mice (n=7–15) were tested for motor coordination in the swimming tank, by assessing the latency to swim over a 60-cm distance to a visible escape platform. Transgenic mice displayed swimming impairments given by a significant increase in the time spent to cross the 60-cm distance. Rotarod analysis of CMVMJD135 and wt animals were tested in (B) an accelerating rod (4–40 rpm) and (C) at constant speeds. The mean±SEM of the latency to fall at each speed level was recorded. Rotarod deficit was present at 20 weeks of age and older (shown for 40 weeks); CMVMJD135 transgenic mice displayed a progressive decline in performance on the rotarod with increasing rotation speed. *p<0.05, **p<0.01, ***p<0.001

the dentate nuclei, locus coeruleus and the cuneate nuclei. The evaluation of cell morphology by cresyl violet staining at 24 weeks of age showed an increased abundance of seemingly atrophic and hyperchromatic neurons in the pontine nuclei of CMVMJD135 mice (Fig. 6C,g–j).

17-DMAG Chronic Treatment Improved Several Features of the Motor Phenotype Observed in CMVMJD135 Mice

Given previous results suggesting that Hsp90 inhibition could be a useful therapeutic approach for polyQ disease, our own finding with 17-DMAG in a nematode model of MJD [32], and the lack of studies in vertebrate models of this disorder, we tested the effect of 17-DMAG in the CMVMJD135 mouse. All analyses in this pre-clinical trial were performed using male mice.

A pilot study was performed in wt animals in order to determine the effective dose of 17-DMAG which induces Hsp70 in the brain. Previous studies have shown increased oral availability of 17-DMAG in comparison with 17-AAG; however, above 10 mg/kg 17-DMAG has been described to be toxic in mice [33]. It has also been demonstrated that i.p. 17-DMAG administration leads to a better bioavailability than the oral route [24]. In our dose–response study using three i.p. injections per week on alternate days, with 17-DMAG at 5, 10 or 25 mg/kg, we observed that, 12 hours post-last injection, only with the dose of 25 mg/kg was the expression of Hsp-70 significantly induced in the brain, this dosage being thus selected for the chronic therapeutic study (Supplementary Fig. 4). With systemic administration of this dosage, the concentration of 17-DMAG in the brain 1 hour after treatment was 42 ng/g (drug quantity/brain weight) with a plasma/brain ration of 0,2.

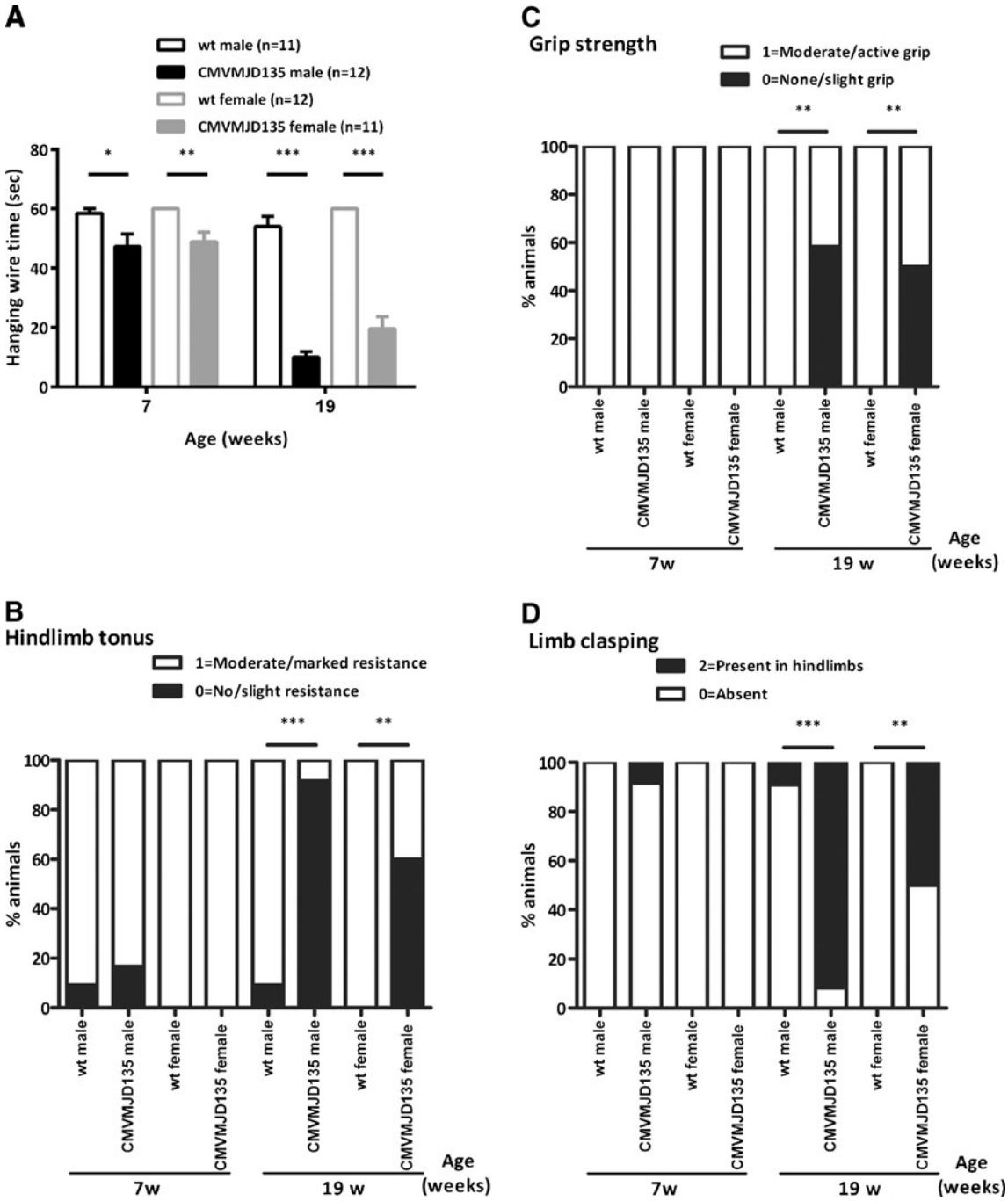

Fig. 5 Phenotype of CMVMJD135 mice detected in the SHIRPA protocol. (A) Strength and fine motor coordination evaluation in the hanging wire grip test, measured by the latency to fall off the grid. Values are presented as mean ± SEM (n=11–12 for each group). (B) At 19 weeks of age animals demonstrated hindlimb tonus alterations, (C) a decrease in forelimb grip strength and (D) a higher percentage of animals displaying clasping of the hindlimbs when compared to controls. Values are presented as percentage of animals with different scores in the SHIRPA protocol (n=11–12 for each group). *p<0.05, **p<0.01, ***p<0.001

In the therapeutic assay, we used four groups of animals: 17-DMAG- and vehicle-treated wt (n=10; n=10, respectively) and CMVMJD135 animals (n=10; n=12, respectively). In the motor swimming test, 17-DMAG treatment had a highly beneficial effect, being able to improve the phenotype of the transgenic animals almost to the performance level of wt animals at 16, 22 and 24 weeks of age (genotype x treatment, $F_{1,38}$=19.912, p=0.00007); this effect was lost at 30 weeks of age (Fig. 7A). 17-DMAG treatment also had a positive effect in the rotarod performance of CMVMJD135 animals, which was comparable to that of wt animals at 22 weeks of age (15 rpm: genotype x treatment, $F_{1,33}$=6.378, p=0.017); this

A

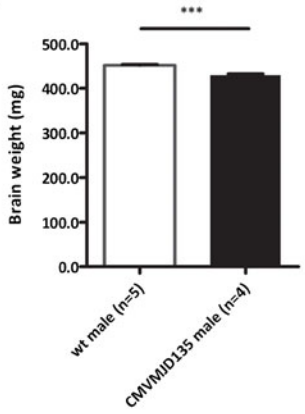

B

Genotype (n)	Brain region	Mean of total volume (µm³) E+08 ± SD E+07	Mean of total cell number (±SD) E+04 ± SD E+03
wild-type (5)	Pontine nuclei	6,47 ±0,752	33,5 ± 41,3
CMVMJD135 (9)		**5,63 ±4,15***	**29,3 ± 24,0***
wild-type (4)	Dentate nuclei	1,45 ± 2,56	7,25 ± 3,94
CMVMJD135 (4)		**0,920 ± 1,01***	6,11 ± 8,81
wild-type (5)	Locus coeruleus	0,294 ± 0,569	2,49 ± 6,67
CMVMJD135 (5)		0,255 ± 0,496	2,09 ± 5,37
wild-type (5)	Substantia nigra	9,75 ± 12,1	40,4 ± 82,7
CMVMJD135 (5)		9,14 ± 16,7	39,9 ± 65,2

C

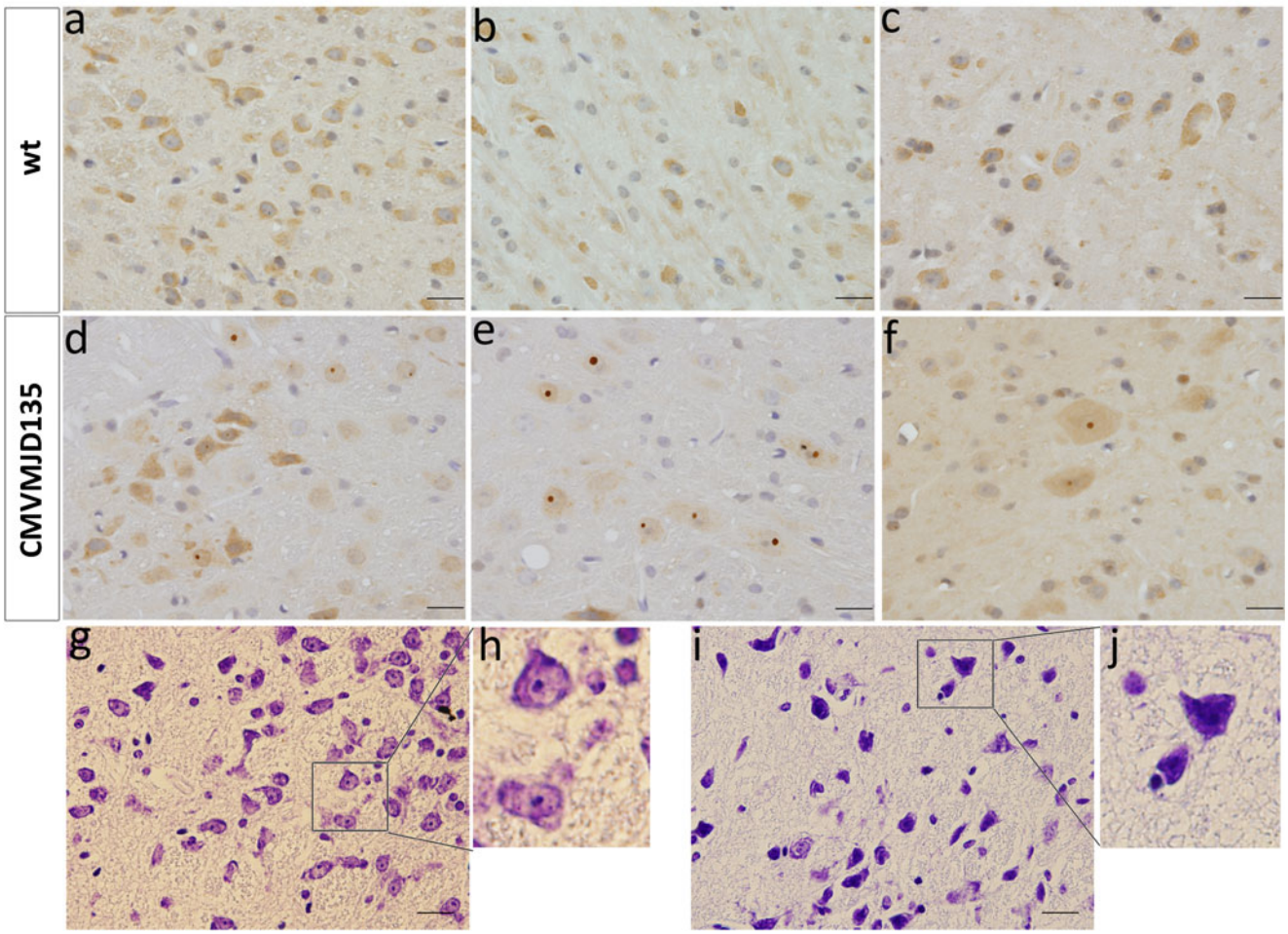

Fig. 6 Neuropathology of CMVMJD135 mice. (A) Brain weight analysis at 42–43 weeks of age of wt (n=5) and CMVMJD135 male mice (n=4). (B) Volume and total cell number quantification in different brain regions of transgenic (n=9) and control (n=5) male animals using stereological methods. (C) Anti-ataxin-3 immunohistochemistry (rabbit anti-MJD1.1) of wt (a-c) and CMVMJD135 mice (d-f) at approximately 20–35 weeks of age. CMVMJD135 mice exhibited nuclear and cytoplasmic inclusions positive for ataxin-3 in different regions of the CNS, namely, pontine nuclei (d), reticulotegmetal nucleus of pons (e) and spinal cord neurons (f); Cresyl violet brain sections in the pontine nuclei of wt (g) and in CMVMJD135 (i) mice. Higher magnification of neuronal cells in the wt (h) and transgenic mice (j). Images are representative of the results obtained for six animals per genotype, three each female and male. Scale bar: 20 µm

effect was no longer statistically significant at 24 and 30 weeks of age (Fig. 7B). At 22 and 24 weeks of age 17-DMAG-treated CMVMJD135 mice had a better performance in the balance beam test (Fig. 7C; Medium square 24 weeks—genotype: $F_{1,37}$=6.228, p=0.017; treatment: $F_{1,37}$=6.903, p=0.012. Small circle 22 weeks—genotype: $F_{1,37}$=7.45, p=0.01;

treatment: $F_{1,37}$=10.385, p=0.003. Small circle 24weeks—genotype: $F_{1,36}$=8.50, p=0.006; treatment: $F_{1,36}$=7.346, p=0.01), which was not maintained at 30 weeks of age, suggesting that 17-DMAG treatment is delaying the manifestation of loss of balance in these animals. Moreover, 17-DMAG was able to delay the onset and progression of the foot-dragging phenotype, since at any age the percentage of CMVMJD135 animals treated with 17-DMAG showing foot-dragging was less than in those not receiving treatment (p<0.05) (Fig. 7D). In summary, 17-DMAG chronic treatment was able to delay the motor deficits in the rotarod, motor swimming and balance beam test by approximately 8 weeks, which represents approximately 9 % of the median C57Bl/6 normal lifespan [34] (600 days), and to a lesser extent the foot-dragging (6 weeks, 7 % of the lifespan).

17-DMAG treatment failed to ameliorate other manifestations of the disease evaluated in the SHIRPA protocol, namely, those more related to weakness/hypotonia (hanging wire, hindlimb tonus), tremors and abnormal reflexes (limb clasping). Although we did not detect any improvement in the hanging wire test, in the total number of rears and body weight, the sample size we used (n=10–12) would be sufficient to detect an improvement of 50 % at several time points (see Supplementary Table). For the number of squares travelled in the arena, the required sample size for the observed mean difference to be significant would be much larger than the one we used (see Supplementary Table).

17-DMAG Treatment Reduces Neuropathology in the CNS of CMVMJD135 Mice

Transgenic vehicle-treated animals demonstrated the presence of shrunken and morphologically abnormal cells in the pontine nuclei. In contrast, 17-DMAG treated animals showed normal cell morphology, shrunken cells being almost undetectable in this brain region at 30 and 16 weeks of age (Supplementary Fig. 5). Quantification of the ataxin-3 nuclear inclusions present in the pontine nuclei of CMVMJD135 mice revealed a significant reduction of the number of cells containing these inclusions, also reflected in a reduced number of inclusions per area, in 17-DMAG-treated transgenic animals when compared to vehicle-treated ones (p=0.009) (Fig. 8A).

Mutant Ataxin-3 Levels are Reduced Through Autophagy in 17-DMAG-Treated CMVMJD135 Mice

No differences were found in ataxin-3 expression at mRNA level in the brainstem between the treatment groups, which allow us to conclude that 17-DMAG treatment is not affecting expression of ataxin-3 at the transcription level (Fig. 8B). Interestingly, however, the protein levels of mutant human ataxin-3 in the brainstem were dramatically reduced in 17-DMAG-treated animals at 16 (p=0.033) and 30 weeks of age (p=0.019), suggesting that this treatment is promoting mutant ataxin-3 degradation rather than refolding (Fig. 8C).

In an attempt to dissect the mechanism of action of the drug we analysed the levels of molecular chaperones in treated animals. Unexpectedly, at 20 weeks, mRNA expression levels of molecular chaperones Hsp-70 and −40 were not significantly increased upon 17-DMAG treatment in transgenic mice, while there was a trend towards increase in the controls (Fig. 9A). Hsp70 quantification in the forebrain at 16 and 30 weeks of age in CMVMJD135 mice demonstrated that chronic treatment with 17-DMAG led to a statistically non-significant trend towards increase in Hsp70 expression in this brain region in transgenic mice at 16 weeks of age, whereas at 30 weeks the opposite trend was present (Fig. 9B). These results suggest that HSR induction by chronic administration of 17-DMAG at 25 mg/kg may be compromised in the disease state, particularly at later stages. Since it was previously shown that 17-AAG and its analogue 17-DMAG are able to activate macroautophagy in different model systems [35–37], we also assessed activation of this pathway. We observed an increase in the beclin-1 protein levels in the brainstem of 16- and 30-week-old mice and of the LC3-II/LC3-I ratio at 30 weeks of age, after chronic 17-DMAG treatment (p=0.008, p=0.017, respectively) in transgenic mice but not in controls, confirming the specificity of this activation (Fig. 9C,D).

Discussion

The pathogenic mechanism of MJD, as well as of other polyQ disorders, is not well understood, and these disorders remain incurable to date. In this work, we have generated a new transgenic mouse model expressing at near the same cDNA variant of ataxin- 3 as in our previous CMVMJD94 model, ATXN3c- which corresponds to the most predominant variant of the protein in the brain [38], but with an increased number of glutamine residues (135Q). Moreover, we tested a potent Hsp90 inhibitor, 17-DMAG, that was able to improve the motor phenotype and the neuropathological features of CMVMJD135 mice.

Our results show that the CMVMJD135 mouse is a powerful model for pre-clinical trials in MJD. The behavioral evaluation of CMVMJD135 mice revealed the presence of several phenotypic abnormalities that gradually appear and progress during a lifespan of over one and a half years, namely, balance and motor coordination deficits, loss of limb strength, decreased locomotor and exploratory activity, abnormal gait and tremors, with many parameters assessable by objective tests. The first sign of neurological disease in the CMVMJD135 model was the presence of balance and grip abnormalities at 6 weeks of age. Cerebellar ataxia is one of the first clinical manifestations seen in MJD patients, and is due to unsteadiness or impaired balance. Although behavioral

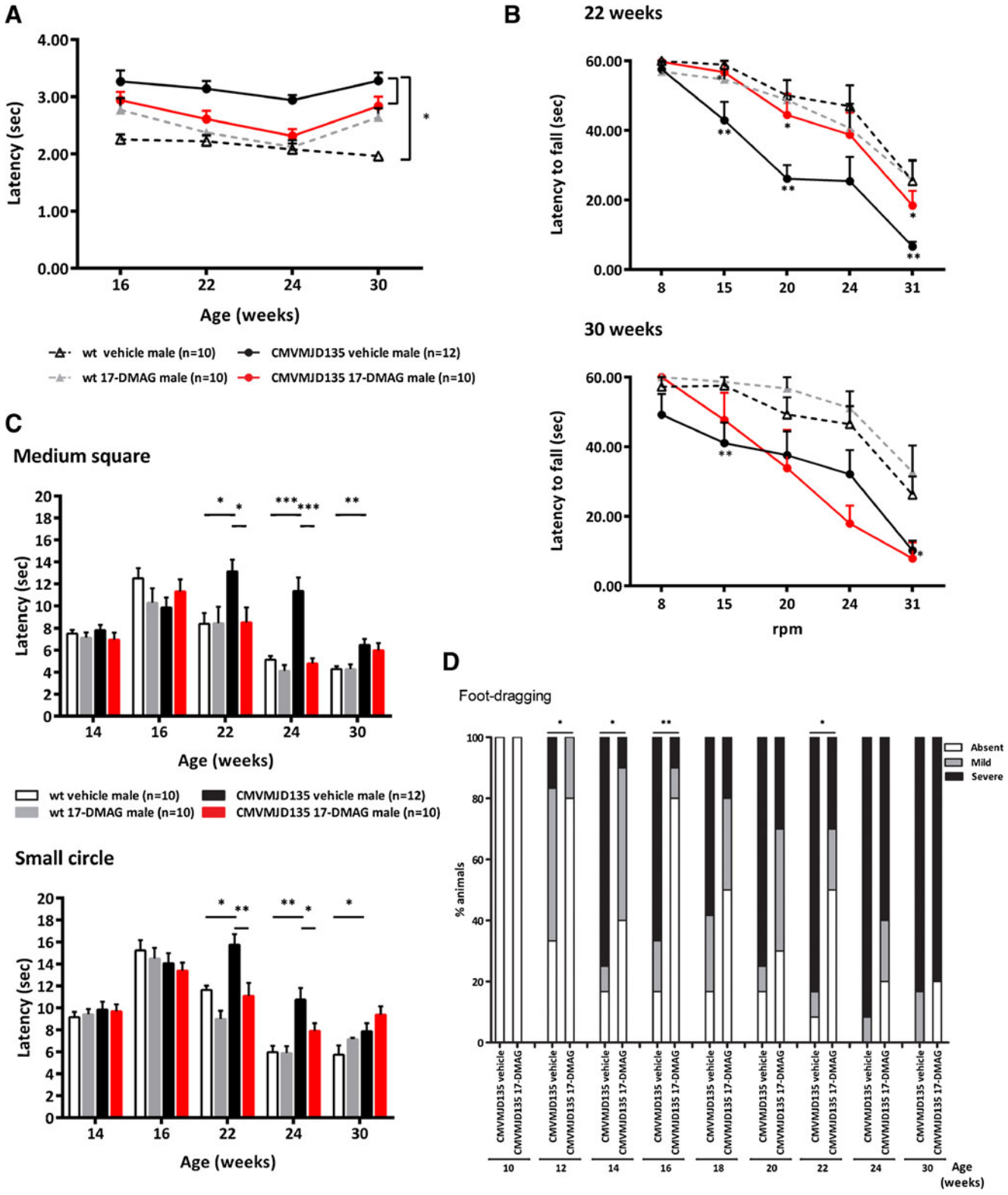

alterations suggestive of loss of coordination in CMVMJD135 mice were observed at 4 and 8 weeks of age, at these ages animals were indistinguishable from their wt littermates by simple observation in their home cage. At 16 weeks of age, however, signs of neurological abnormality were already observable in CMVMJD135 mice in their home cage, in particular a clearly abnormal gait. The footprinting pattern evaluation of CMVMJD135 mice clearly demonstrated foot-

◀ **Fig. 7** 17-DMAG improves motor coordination of CMVMJD135 mice. (A) Motor swimming test was performed at 16, 22, 24 and 30 weeks of age (n=10–12 animals for each tested group) and the mean latency of the third day test was analyzed. Transgenic mice displayed swimming impairments, given by a significant increase in the time spent to swim across 60 cm distance, and 17-DMAG treatment improved their performance. (B) Rotarod test was performed at 22 and 30 weeks of age (n=10–12 for each tested group) to evaluate motor coordination at constant speed in the rod (8, 15, 20, 24 and 31 rpm). 17-DMAG treatment was able to rescue this phenotype at 22 weeks of age. (C) Balance beam test was performed at 14, 16, 22, 24 and 30 weeks of age (n=10–12 for each tested group. 17-DMAG treatment significantly improved balance deficits at 22 and 24 weeks of age. Values are presented as mean ± SEM. (D) Quantitative analysis of the percentage of animals showing foot-dragging. 17-DMAG treatment delays the onset and progression of this symptom. *p<0.05, **p<0.01, ***p<0.001

dragging and, at later stages of the disease, a shortened step length and a decrease in the hind/ frontlimb overlap. Transgenic animals also showed a significant deficit in the accelerating rod at 20 weeks of age, which was further aggravated at 40 weeks of age, in the constant and accelerating rod. In the motor swimming test, the abnormal posture and inappropriate kicking movements exhibited by CMVMJD135 contrasted markedly with the coordinated synchronized paddling movements shown by wt mice.

The analysis of CAG repeat number through the generations of CMVMJD135 mice revealed that CAG tract length varied in approximately 54–79 % of the transmissions, frequently towards contractions. The genescan profile of the CAG tract obtained from mouse tail revealed that somatic mosaicism was also present. Thus, our new model seems to replicate this feature of the human disease as well.

The histological evaluation of CMVMJD135 mouse brains frequently revealed abnormal cell morphology in the pontine nuclei as well as gliosis in the substantia nigra at clearly symptomatic ages (24 weeks of age). The stereological analysis of pontine nuclei of CMVMJD135 brain at late stages (60 weeks of age) revealed a reduced volume and total cell number in this region and reduced volume in the dentate nuclei, two regions of high involvement in human patients. Moreover, we observed a total brain weight decrease, but only at late stages of the disease (42–43 weeks of age), which supports the hypothesis that major cell loss only occurs at these advanced stages. These results suggest that the early motor phenotype observed in our model is mostly attributable to dysfunction of the brain regions affected in MJD, clearly preceding neuronal cell death. In order to validate this hypothesis, it will be necessary to perform a longitudinal neuropathology analysis of the brain regions affected in MJD, to

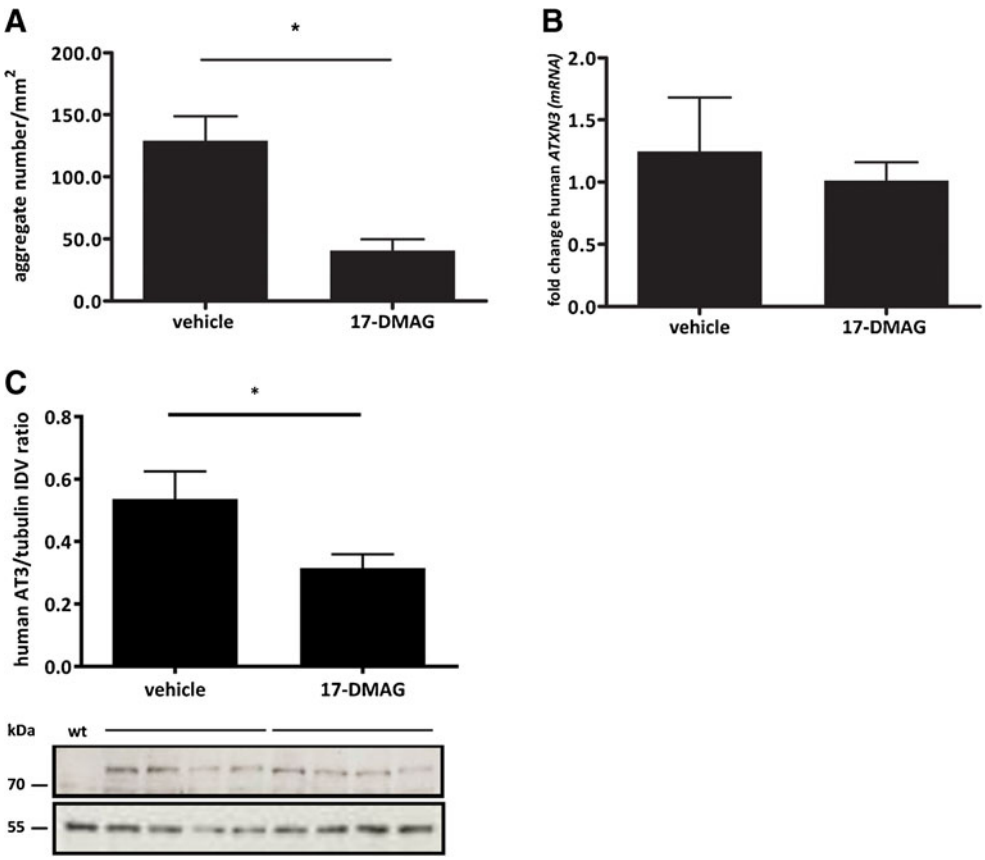

Fig. 8 17-DMAG treatment reduced the levels of human ataxin-3 and the aggregate load in CMVMJD135 mice brain. (A) Neuronal inclusions were counted in the pontine nuclei of 30-week-old animals treated with vehicle or 17-DMAG (n=3 for each condition). Four slides of each animal were used for the analysis. (B) qRT-PCR analysis of human ATXN3 mRNA expression levels (n=4). (C) Anti-ataxin-3 western-blot (rabbit anti-MJD1.1) of 30-week-old CMVMJD135 mice, either vehicle or treated with 17-DMAG (n=4 for each condition), were performed in the brainstem. Mutant human ataxin-3 has a molecular weight of approximately 80 kDa. Values are presented as mean ± SEM; *p<0.05, **p<0.01, ***p<0.001

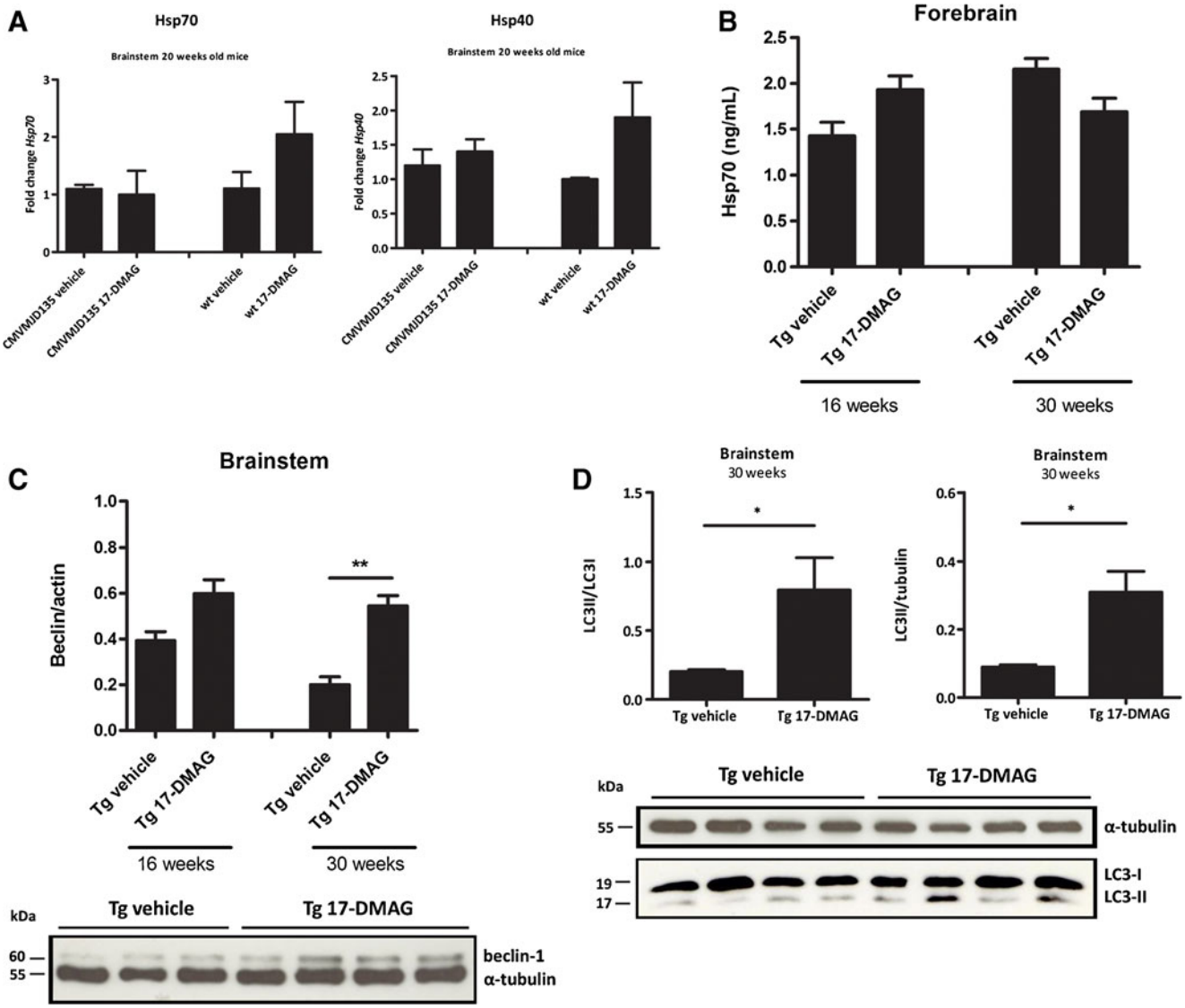

Fig. 9 17-DMAG is able to induce autophagy in CMVMJD135 animals. ELISA assays, western blots and qRT-PCR analysis of HSR and autophagy markers were performed in the brainstem or forebrain of 16-, 20- or 30-week-old wt and CMVMJD135 mice (n=4–5) treated with vehicle or 17-DMAG (25 mg/kg), 12 hours after the last treatment. (A) *Hsp70*, *Hsp40* mRNA expression levels were normalized for the housekeeping gene *HPRT*. (B) ELISA assay for Hsp70 quantification. Anti- Beclin-1 (C) and anti-LC3 (D) western-blots. LC3-II was normalized both for tubulin and LC3-I; Beclin-1 was normalized for tubulin. Values are presented as mean ± SEM; *p<0.05, **p<0.01, ***p<0.001

establish correlations between the phenotype here defined and the neurodegeneration pattern.

An important feature of MJD, as well as of other polyQ diseases, is the presence of neuronal inclusions containing the mutant protein. Our previous results have shown the presence of motor symptoms in a transgenic mouse model of MJD in the absence of intranuclear inclusions, suggesting that these are not essential for disease manifestation [31]. However, the nature and relevance of intermediate species of the aggregation process remains to be elucidated in this disorder. In this new transgenic mouse, intranuclear inclusions were present in the cells of affected brain regions, such as the pontine and deep cerebellar nuclei, but also in regions that are spared, such as the anterior olfactory nuclei and ventral tenia tecta. This is concordant with what is seen in human MJD patients, where neurodegeneration was not clearly correlated with the occurrence of ataxin-3 immunopositive inclusions [39]. Moreover, neuronal inclusions were observed already at 20 but not at 16 weeks of age, when several motor symptoms were already clearly present. This is in agreement with previous results obtained in other transgenic mouse models of MJD, in which symptoms appear before the detection of the inclusions [40].

Although the role of intranuclear inclusions, the end-product of the aggregation process in MJD pathogenesis, remains to be clarified, the presence of this pathological hallmark of disease in our model indicates that it successfully replicates the full aggregation process that happens in humans. The combination of clinical and neuropathologic features of

CMVMJD135 mice prompted us to start pre-clinical trials using different compounds, targeting different potential pathogenic mechanisms for MJD.

The chaperone machinery has the potential to neutralize the toxicity caused by misfolded and aggregated proteins, making the activation of molecular chaperones an attractive therapeutic strategy [21, 41]. Treatment of CMVMJD135 mice with 17-DMAG markedly improved motor performance, given by the results in the motor swimming, rotarod and beam balance tests, reduced the expression levels of human ataxin-3 at protein level and reduced the nuclear aggregate load in the pontine nuclei. Regarding neuropathology, 17-DMAG also led to a visible amelioration in cell morphology in affected brain areas, such as the pontine nuclei, at 16 and 30 weeks of age. Intriguingly, however, 17-DMAG had no beneficial effect in other neurological symptoms, for instance, limb weakness, tremor and abnormal reflexes, and the beneficial effects of 17-DMAG treatment were not maintained throughout disease progression. At 30 weeks of age, CMVMJD135 mice treated with 17-DMAG started to present MJD symptoms similar to those of mice treated with saline. Data from preclinical toxicity studies for 17-DMAG in animal models have recently become available [33], leading us to believe that it is possible to further increase 17-DMAG dose (higher than 25 mg/kg) while keeping outside its toxicity range; this should be tested in future studies.

In our study, and in spite of the therapeutic effects observed, the chronic administration of 17-DMAG failed to induce the HSR in CMVMJD135 mice, particularly at later stages of the disease. This is in agreement with what was recently described in a Huntington's disease mouse model treated with an Hsp90 inhibitor [42]. These authors tested the effectiveness of HSF-1 dissociation from the Hsp90 complex, its translocation to the nucleus and consequent hyperphosphorylation, features interfering with HSF-1 trimerization and its ability to induce HS gene expression [43], and concluded that all those processes were occurring normally upon treatment, suggesting that the problem was at the level of transcriptional activation of HSF1 targets due to excessive chromatin condensation. A similar phenomenon appears to be taking place in CMVMJD135 mice.

Since it was previously shown that 17-AAG and its analogue used in this study—17-DMAG—are able to activate the autophagy process in different model systems [35–37], and given that our results suggested degradation of ataxin-3 was occurring, we assessed known autophagy markers in 17-DMAG-treated animals. Our results suggest that autophagy is activated by the drug specifically in diseased animals. This is confirmed by an increase in the protein levels of Beclin-1 and LC3-II, detected only in 17-DMAG-treated CMVMJD135 mice. Although we could not observe an induction of HS genes at the age tested (20 and 30 weeks of age), this induction might still happen earlier in life, being no longer seen in later disease stages, when autophagy starts taking place as a compensatory mechanism. In addition to improving the major symptoms of disease, 17-DMAG reduced mutant protein levels and aggregate load in CMVMJD135 mice, which is a good additional proof of its beneficial effects. 17-DMAG is currently in Phase I of clinical trials for advanced solid tumors (www.clinicaltrials.gov), to test dosage, toxicity, pharmacokinetics and pharmacodynamics. So far, the most frequently observed collateral effects of this compound were fatigue, nausea, diarrhea and headache [44]. Although the effects of continuous activation of HSF-1 are not well understood, and it was suggested to be detrimental in some situations [45], our data show that 17-DMAG is a promising compound and Hsp90 an interesting molecular target for MJD therapy. There is a need to better understand the impairment of the HSR during aging in mice (since this study is not easy to perform in humans) which will help in the development of new drugs that can act synergistically with 17-DMAG in the improvement of proteostasis.

Materials and Methods

Generation of Transgenic Mice, Breeding, Genotyping, CAG Repeat Sizing and Mouse Maintenance

To generate transgenic MJD mice, we converted the ATXN3a cDNA variant carrying a repeat tract ($(CAG)_2CAAAAGCAGCAA(CAG)_{124}$), coding for 130 glutamines (plasmid pF25B3.3::AT3Q130::YFP) in the ATXN3c variant [18] into the pCMV vector (Fig. 1A). This plasmid, designated pCMVAT3Q135_1.5, was linearized by total digestion with PaeI (Fermentas), the fragment of interest (3150 bp) was then purified from an agarose gel using the QiaQuick gel extraction system (Qiagen, Hamburg, Germany) and microinjected into fertilized murine oocytes of the C57Bl/6 mouse strain (QTRN, Canada). To establish the lineage CMVMJD135, founder C was bred with C57Bl/6 females and the hemizygous progeny were bred with littermate wt animals to generate the experimental groups. DNA extraction, animal genotyping, transgene copy number and CAG repeat size analyses were performed as previously described [31].

All animal procedures were conducted in accordance with European regulations (European Union Directive 86/609/EEC). The animals were anesthetized with a mixture of ketamine hydrochloride (150 mg/kg) plus medetomidine (0.3 mg/kg). Animal facilities and the people directly involved in animal experiments (ASF, SDS, ANC) were certified by the Portuguese regulatory entity — Direcção Geral de Veterinária. All of the protocols performed were approved by the joint Animal Ethics Committee of the Life and Health Sciences Research Institute, University of Minho, and the Institute for

Molecular and Cell Biology, University of Porto. Health monitoring was performed according to FELASA guidelines [46], confirming the Specified Pathogen Free health status of sentinel animals maintained in the same animal room.

Behavioral Analysis

CMVMJD135 phenotypic characterization was performed during the diurnal period in groups of five animals per cage including CMVMJD135 hemizygous transgenic mice and wt littermates (n=11–15 per genotype and gender). The mean repeat size (±SD) for all mice used was (133±1). Animals were evaluated monthly in the rotarod [31] (beginning at 4 weeks of age until 40 weeks of age), by the modified SHIRPA protocol [31] (at 7, 19 and 40 weeks of age), using the balance beam test [47] (at 10 and 22 weeks of age) and the motor swimming test [47] (between 22–25 and 40 weeks of age). Rotarod tests and footprinting pattern were performed as previously described [31] as was the SHIRPA protocol, with the addition of the hanging wire grip test. To evaluate the severity of foot-dragging through age the footprinting patern of CMVMJD135 (n=10) and wt controls (n=7) was classified at each time point considering six consecutive steps (0=absent/mild, up to three steps; 1=moderate, more than three steps out of six; 2=severe, all steps out of six).

Hanging Wire Grip Test Each mouse was placed on a wire cage top, which was slowly inverted and suspended at approximately 30 cm to the floor. The time it took each mouse to fall from the cage top was recorded. Any mouse still gripping the cage top after 60 seconds was removed.

Balance Beam Test Motor coordination and balance of mice were assessed by measuring the ability of the mice to traverse a graded series of narrow beams to reach an enclosed safety platform as previously described [47]. The beams consisted of long strips of PVC (1 m) with a 27- and 11-square cross-section or a 28-, 15-, or 10-mm round diameter. During training, mice were placed at the start of the 11-mm square beam and trained over 3 days (3 trials per day) to traverse the beam to the safe platform.

Motor swimming test [47] and Morris water maze were performed as previously described [48, 49].

Western Blot

Protein isolation from mouse tissues and western blot were performed as previously described [31] homogenized in cold RIPA buffer and a mixture of protease inhibitors (Complete; Roche). The blots were blocked overnight at 4 °C with the primary Ab: rabbit anti-ataxin-3 serum (kindly provided by Dr. Henry Paulson) (1:10000); mouse anti-Hsp70 (1:2000 StressGene), rabbit anti-LC3 (1:500 Cell Signaling), rabbit anti-Beclin1 (1:1000 Cell signaling) and mouse anti-alpha-tubulin (1:100, DSHB). Band quantification was performed using ImageJ software according to the manufacturer's instructions using alpha-tubulin as the loading control.

qRTPCR

Total RNA was isolated from CMVMJD135 mice tissues using TRIZOL (Invitrogen, Calrsbad, CA, USA) according to the manufacturer's protocol. First-strand cDNA, synthesized using oligo-dT (Bio-rad), was amplified by quantitative reverse-transcriptase PCR (qRT-PCR) as previously described [31]. Human and mouse ataxin-3 primers were used for transgene expression quantification [31]: HSP40 (F: 5'CGCCGG ACGGGTATATAGAG3'; R: 5'GGCCCAGCGTCTGATA GTAG3'), HSP70 (F: 5'CCAACGCTGTCACTCAAACC 3'; R: 5'GCCCTTGTCCAGAACTCTCC3') and LC3 (F: 5'TTCTTCCTCCTGGTGAATGG3'; R: 5'GTGGGTGCCT ACGTTCTCAT3').

Neuropathology and Immunohistochemistry

Transgenic and wt littermate mice were deeply anesthetized and transcardially perfused with PBS followed by 4 % paraformaldehyde (PFA) in PBS. Brains were postfixed overnight in fixative solution and embedded in paraffin. Slides with 4-μm-thick paraffin sections were stained with cresyl violet or processed for immunohistochemistry with rabbit GFAP Ab (DAKO Corporation, Carpinteria, CA) (1:500) or rabbit anti-MJD1.1 [50] (1:40) or anti-ubiquitin (1:500) [31]. Ataxin-3 positive inclusions in the pontine nuclei of 30 weeks old animals either vehicle or 17-DMAG treated (n=3–4 for each condition, three slides per animal) were quantified and normalized for total area using the Olympus BX 51 stereological microscope and the Visiopharma integrator system software.

Stereological Analysis Neuronal number and volume were obtained by systematic random sampling in pontine nuclei from Bregma level −3.80 mm through 4.60 mm; substantia nigra from Bregma level −2.46 mm through 4.04 mm; locus coeruleus from Bregma level −5.34 mm through 5.80 mm and dentate nuclei from Bregma level −5.68 mm thourh 6.36, according to the Paxinos and Franklin mouse brain atlas of 2001. Every second section containing the region of interest was selected to obtain a sample in a systematic uniform and random manner (section sampling fraction; ssf = 0.5). Volume estimation was obtained according to Cavalieri's principle [51]. Each known area was multiplied by the represented thickness (30 μm x 2 sections). Average cell numbers were estimated using the optical fractionator method [52]. The area (a) of the counting frame was 400 μm^2 (20 μm x 20 μm), the area sampling fraction (asf) = a (frame)/ a (step length) was

0.004. The height (h: 15 μm) of the optical dissector was equivalent to the thickness of the section (t: 30 μm).

The measurements were performed using The Visiopharm Integrator System, version 2.12.3.0 and a camera (Pixelink PL-A622) attached to a motorized microscope (Olympus BX51).

17-DMAG Dose Determination

Wt animals were injected with 17-DMAG (InvivoGen) at different concentrations (5, 10 and 25 mg/kg, n=4 per dose) three times per week on alternate days, and 12 hours after the last injection the animals were sacrificed. Another set of animals (n=4) was injected with vehicle (saline NaCl 0,9 %) and sacrificed at the same time. The protein levels of Hsp70 were measured by western blot in the muscle and in the brain.

Determination of Blood/Plasma Ratio to Estimate 17-DMAG brain exposure

A total of six C57Bl/6 mice at approximately 6 months of age were used, in which two were injected intraperitoneally three times in a week with saline—0.9 % NaCl and four animals with 17-DMAG 25 mg/kg. Animals were anesthetized 1 hour post-injection and the blood was removed from the inferior vena cava, and after perfusion with PBS brains were dissected, weighted and immediately frozen at −80ºC. Brain tissue was homogenized in acetonitrile:H_20 (4:1 v/v). After centrifugation, plasma and brain supernatants were harvested and samples were frozen at −80 °C until bioanalysis. Brain and plasma samples were analysed for content of drug by use of UltraPerformance LC® (UPLC®) chromatography followed by tandem-MS (MS/MS) detection.

Hsp70 ELISA Assay

An Hsp70 ELISA kit (ADI-EKS-700B from ENZO life sciences, UK) was used to measure the Hsp70 concentration in brain tissue from mice. The analysis was carried out according to the manufacturer's instructions. Briefly, forebrain tissue protein extracts were obtained as described above and extraction reagent (ELISA kit) with phosphostop and protease inhibitor cocktail was added. The homogenate was spinned down at 20,000 g for 10 min and the supernantant was kept at −80 °C until analysis. The protein concentration was determined using a standard BCA Protein assay (Thermo scientific, Denmark), and upon ELISA analysis, 100 μg of protein was analysed per well according to the standard protocol. The developed plates were measured with a Spectramax 340PC (Molecular Devices Inc., USA) at 450 nm (reference 540 nm). Hsp70 concentration was calculated based on the standard curve and expressed as ng of Hsp70 per ml.

17-DMAG Treatment and Behavioral Assessment

CMVMJD135 and littermate mice (n=10−12 for each group) were intraperitoneally injected three times a week since 5 weeks of age (one week before the onset of symptoms) with 17-DMAG at 25 mg/kg (for a mean mouse weight of 25 g) or with a 0.9 % saline solution. The animals were evaluated every two weeks in the balance beam test and using the SHIRPA protocol since 6 weeks of age. Foot-dragging was evaluated as described above and at the age of 16, 22, 24 and 30 weeks the animals were also tested in the rotarod and in the motor swimming test. Behavior analysis methods were described above.

Statistical Analysis

Power analysis was used to determine the sample size [53]. Considering the different variables under study, such as weight, time held in the hanging wire, rotarod and swimming latency, assuming a power of 0.8 and a significance level of 0.05, different required sample sizes were obtained, depending on the specified smallest detectable difference and the variability within the four populations under study (wt vehicle, wt 17-DMAG, tg vehicle and tg 17-DMAG). Based on these calculations and bearing in mind that as the age of the animals increases also the mean differences increase and, possibly, the standard deviations, a sample size ranging between five and ten animals was obtained and, therefore, a sample of ten animals was chosen. Sample size calculations of each behavioral test were also assessed assuming a power of 0.8 and a significance level of 0.05 (Supplementary Table). The effect size was calculated taking into account an improvement of 50 %, using mean and standard deviation values previously obtained for transgenic and control groups for the different behavioral tests.

Behavioral data were analyzed by the non-parametric Mann–Whitney U-test when variables were non-continuous or when a continuous variable did not present a normal distribution (Kolmogorov-Smirnov (K-S) test $p<0.05$). Continuous variables with normal distributions (K-S test $p>0.05$) were analyzed with the Student's t-test and two-way ANOVA (factors: genotype and age for basal behavioral characterization of the CMVMJD135 mice; factors: genotype and treatment in the 17-DMAG preclinical trial). For the motor swimming test, repeated-measures ANOVA was performed considering two factors: genotype and treatment. All statistical analyses were performed using SPSS 22.0 (SPSS Inc., Chicago, IL). A critical value for significance of two-tailed $p<0.05$ was used throughout the study.

Acknowledgements We would like to thank to Dr. Henry Paulson for providing the anti-ataxin-3 serum, Dr. Mónica Sousa for the pCMV vector and to Eng. Lucília Goreti Pinto, Luís Martins, Miguel Carneiro and Celina Barros for technical assistance. This work was supported by Fundação para a Ciência e Tecnologia through the projects FEDER/FCT, POCI/SAU-MMO/60412/2004 and PTDC/SAU-GMG/64076/2006.

This work was supported by Fundação para a Ciência e Tecnologia through fellowships SFRH/BPD/91562/2012 to A.S-F., SFRH/BD/78388/2011 to S.D-S., SFRH/BD/51059/2010 to A.N-C., and SFRH/BPD/79469/2011 to A.T-C..

References

1. Maciel P, Costa MC, Ferro A, Rousseau M, Santos CS, Gaspar C et al. Improvement in the molecular diagnosis of Machado-Joseph disease. Arch Neurol. 2001;58(11):1821–7.
2. Coutinho P, Andrade C. Autosomal dominant system degeneration in Portuguese families of the Azores Islands. A new genetic disorder involving cerebellar, pyramidal, extrapyramidal and spinal cord motor functions. Neurology. 1978;28(7):703–9.
3. Seidel K, den Dunnen WF, Schultz C, Paulson H, Frank S, de Vos RA et al. Axonal inclusions in spinocerebellar ataxia type 3. Acta Neuropathol. 2010;120(4):449–60.
4. Paulson HL, Perez MK, Trottier Y, Trojanowski JQ, Subramony SH, Das SS et al. Intranuclear inclusions of expanded polyglutamine protein in spinocerebellar ataxia type 3. Neuron. 1997;19(2):333–44.
5. Huang S, Ling JJ, Yang S, Li XJ, Li S. Neuronal expression of TATA box-binding protein containing expanded polyglutamine in knock-in mice reduces chaperone protein response by impairing the function of nuclear factor-Y transcription factor. Brain. 2011;134(Pt 7):1943–58.
6. Zijlstra MP, Rujano MA, Van Waarde MA, Vis E, Brunt ER, Kampinga HH. Levels of DNAJB family members (HSP40) correlate with disease onset in patients with spinocerebellar ataxia type 3. Eur J Neurosci. 2010;32(5):760–70.
7. Chai Y, Koppenhafer SL, Bonini NM, Paulson HL. Analysis of the role of heat shock protein (Hsp) molecular chaperones in polyglutamine disease. J Neurosci. 1999;19(23):10338–47.
8. Williams AJ, Knutson TM, Colomer Gould VF, Paulson HL. In vivo suppression of polyglutamine neurotoxicity by C-terminus of Hsp70-interacting protein (CHIP) supports an aggregation model of pathogenesis. Neurobiol Dis. 2009;33(3):342–53.
9. Yoshida H, Yoshizawa T, Shibasaki F, Shoji S, Kanazawa I. Chemical chaperones reduce aggregate formation and cell death caused by the truncated Machado-Joseph disease gene product with an expanded polyglutamine stretch. Neurobiol Dis. 2002;10(2):88–99.
10. Warrick JM, Chan HY, Gray-Board GL, Chai Y, Paulson HL, Bonini NM. Suppression of polyglutamine-mediated neurodegeneration in Drosophila by the molecular chaperone HSP70. Nat Genet. 1999;23(4):425–8.
11. Kaushik S, Cuervo AM. Chaperones in autophagy. Pharmacol Res. 2012;66(6):484–93.
12. Lamark T, Johansen T. Aggrephagy: selective disposal of protein aggregates by macroautophagy. Int J Cell Biol. 2012;2012:736905.
13. Zou J, Guo Y, Guettouche T, Smith DF, Voellmy R. Repression of heat shock transcription factor HSF1 activation by HSP90 (HSP90 complex) that forms a stress-sensitive complex with HSF1. Cell. 1998;94(4):471–80
14. Kim HR, Kang HS, Kim HD. Geldanamycin induces heat shock protein expression through activation of HSF1 in K562 erythroleukemic cells. IUBMB Life. 1999;48(4):429–33.
15. Hay DG, Sathasivam K, Tobaben S, Stahl B, Marber M, Mestril R et al. Progressive decrease in chaperone protein levels in a mouse model of Huntington's disease and induction of stress proteins as a therapeutic approach. Hum Mol Genet. 2004;13(13):1389–405.
16. Sittler A, Lurz R, Lueder G, Priller J, Lehrach H, Hayer-Hartl MK et al. Geldanamycin activates a heat shock response and inhibits huntingtin aggregation in a cell culture model of Huntington's disease. Hum Mol Genet. 2001;10(12):1307–15.
17. Auluck PK, Meulener MC, Bonini NM. Mechanisms of suppression of {alpha}-synuclein neurotoxicity by geldanamycin in Drosophila. J Biol Chem. 2005;280(4):2873–8.
18. Teixeira-Castro A, Ailion M, Jalles A, Brignull HR, Vilaca JL, Dias N et al. Neuron-specific proteotoxicity of mutant ataxin-3 in C. elegans: rescue by the DAF-16 and HSF-1 pathways. Hum Mol Genet. 2011;20(15):2996–3009.
19. Waza M, Adachi H, Katsuno M, Minamiyama M, Sang C, Tanaka F et al. 17-AAG, an Hsp90 inhibitor, ameliorates polyglutamine-mediated motor neuron degeneration. Nat Med. 2005;11(10):1088–95.
20. Tokui K, Adachi H, Waza M, Katsuno M, Minamiyama M, Doi H et al. 17-DMAG ameliorates polyglutamine-mediated motor neuron degeneration through well-preserved proteasome function in an SBMA model mouse. Hum Mol Genet. 2009;18(5):898–910.
21. Katsuno M, Sang C, Adachi H, Minamiyama M, Waza M, Tanaka F et al. Pharmacological induction of heat-shock proteins alleviates polyglutamine-mediated motor neuron disease. Proc Natl Acad Sci USA. 2005;102(46):16801–6.
22. Ronnen EA, Kondagunta GV, Ishill N, Sweeney SM, Deluca JK, Schwartz L et al. A phase II trial of 17-(Allylamino)-17-demethoxygeldanamycin in patients with papillary and clear cell renal cell carcinoma. Invest New Drugs. 2006;24(6):543–6.
23. Smith V, Sausville EA, Camalier RF, Fiebig HH, Burger AM. Comparison of 17-dimethylaminoethylamino-17-demethoxygeldanamycin (17DMAG) and 17-allylamino-17-demethoxygeldanamycin (17AAG) in vitro: effects on Hsp90 and client proteins in melanoma models. Cancer Chemother Pharmacol. 2005;56(2):126–37.
24. Egorin MJ, Lagattuta TF, Hamburger DR, Covey JM, White KD, Musser SM et al. Pharmacokinetics, tissue distribution, and metabolism of 17-(dimethylaminoethylamino)-17-demethoxygeldanamycin (NSC 707545) in CD2F1 mice and Fischer 344 rats. Cancer Chemother Pharmacol. 2002;49(1):7–19.
25. Chadman KK, Yang M, Crawley JN. Criteria for validating mouse models of psychiatric diseases. Am J Med Genet B Neuropsychiatr Genet. 2009;150B(1):1–11.
26. Costa Mdo C, Paulson HL. Toward understanding Machado-Joseph disease. Prog Neurobiol. 2012;97(2):239–57.
27. Bichelmeier U, Schmidt T, Hubener J, Boy J, Ruttiger L, Habig K et al. Nuclear localization of ataxin-3 is required for the manifestation of symptoms in SCA3: in vivo evidence. J Neurosci. 2007;27(28):7418–28.
28. Cemal CK, Carroll CJ, Lawrence L, Lowrie MB, Ruddle P, Al-Mahdawi S et al. YAC transgenic mice carrying pathological alleles of the MJD1 locus exhibit a mild and slowly progressive cerebellar deficit. Hum Mol Genet. 2002;11(9):1075–94.
29. Chou AH, Yeh TH, Ouyang P, Chen YL, Chen SY, Wang HL. Polyglutamine-expanded ataxin-3 causes cerebellar dysfunction of SCA3 transgenic mice by inducing transcriptional dysregulation. Neurobiol Dis. 2008;31(1):89–101.
30. Goti D, Katzen SM, Mez J, Kurtis N, Kiluk J, Ben-Haiem L et al. A mutant ataxin-3 putative-cleavage fragment in brains of Machado-Joseph disease patients and transgenic mice is cytotoxic above a critical concentration. J Neurosci. 2004;24(45):10266–79.
31. Silva-Fernandes A, Costa Mdo C, Duarte-Silva S, Oliveira P, Botelho CM, Martins L et al. Motor uncoordination and neuropathology in a transgenic mouse model of Machado-Joseph disease lacking intranuclear inclusions and ataxin-3 cleavage products. Neurobiol Dis. 2010;40(1):163–76.
32. Teixeira-Castro A, Ailion M, Jalles A, Brignull HR, Vilaca JL, Dias N et al. Neuron-specific proteotoxicity of mutant ataxin-3 in C. elegans: rescue by the DAF-16 and HSF-1 pathways. Hum Mol Genet. 2011; 20(15):2996–3009.
33. Hollingshead M, Alley M, Burger AM, Borgel S, Pacula-Cox C, Fiebig HH et al. In vivo antitumor efficacy of 17-DMAG (17-

dimethylaminoethylamino-17-demethoxygeldanamycin hydrochloride), a water-soluble geldanamycin derivative. Cancer Chemother Pharmacol. 2005;56(2):115–25.
34. Curtis HJ. Genetic factors in aging. Adv Genet. 1971;16:305–24.
35. Palacios C, Martin-Perez R, Lopez-Perez AI, Pandiella A, Lopez-Rivas A. Autophagy inhibition sensitizes multiple myeloma cells to 17-dimethylaminoethylamino-17-demethoxygeldanamycin-induced apoptosis. Leuk Res. 2010;34(11):1533–8.
36. Rusmini P, Simonini F, Crippa V, Bolzoni E, Onesto E, Cagnin M et al. 17-AAG increases autophagic removal of mutant androgen receptor in spinal and bulbar muscular atrophy. Neurobiol Dis. 2011;41(1):83–95.
37. Riedel M, Goldbaum O, Schwarz L, Schmitt S, Richter-Landsberg C. 17-AAG induces cytoplasmic alpha-synuclein aggregate clearance by induction of autophagy. PLoS One. 2010;5(1):e8753.
38. Harris GM, Dodelzon K, Gong L, Gonzalez-Alegre P, Paulson HL. Splice isoforms of the polyglutamine disease protein ataxin-3 exhibit similar enzymatic yet different aggregation properties. PLoS One. 2010;5(10):e13695.
39. Rub U, de Vos RA, Brunt ER, Sebesteny T, Schols L, Auburger G et al. Spinocerebellar ataxia type 3 (SCA3): thalamic neurodegeneration occurs independently from thalamic ataxin-3 immunopositive neuronal intranuclear inclusions. Brain Pathol. 2006;16(3):218–27.
40. Boy J, Schmidt T, Schumann U, Grasshoff U, Unser S, Holzmann C et al. A transgenic mouse model of spinocerebellar ataxia type 3 resembling late disease onset and gender-specific instability of CAG repeats. Neurobiol Dis. 2010;37(2):284–93.
41. Herbst M, Wanker EE. Small molecule inducers of heat-shock response reduce polyQ-mediated huntingtin aggregation. A possible therapeutic strategy. Neurodegener Dis. 2007;4(2–3):254–60.
42. Labbadia J, Cunliffe H, Weiss A, Katsyuba E, Sathasivam K, Seredenina T et al. Altered chromatin architecture underlies progressive impairment of the heat shock response in mouse models of Huntington disease. J Clin Invest. 2011;121(8):3306–19.
43. Akerfelt M, Morimoto RI, Sistonen L. Heat shock factors: integrators of cell stress, development and lifespan. Nat Rev Mol Cell Biol. 2010;11(8):545–55.
44. Ramanathan RK, Egorin MJ, Erlichman C, Remick SC, Ramalingam SS, Naret C et al. Phase I pharmacokinetic and pharmacodynamic study of 17-dimethylaminoethylamino-17-demethoxygeldanamycin, an inhibitor of heat-shock protein 90, in patients with advanced solid tumors. J Clin Oncol. 2010;28(9):1520–6.
45. Feder JH, Rossi JM, Solomon J, Solomon N, Lindquist S. The consequences of expressing hsp70 in Drosophila cells at normal temperatures. Genes Dev. 1992;6(8):1402–13.
46. Nicklas W, Baneux P, Boot R, Decelle T, Deeny AA, Fumanelli M et al. Recommendations for the health monitoring of rodent and rabbit colonies in breeding and experimental units. Lab Anim. 2002;36(1):20–42.
47. Carter RJ, Lione LA, Humby T, Mangiarini L, Mahal A, Bates GP et al. Characterization of progressive motor deficits in mice transgenic for the human Huntington's disease mutation. J Neurosci. 1999;19(8):3248–57.
48. Morris R. Developments of a water-maze procedure for studying spatial learning in the rat. J Neurosci Methods. 1984;11(1):47–60.
49. Cerqueira JJ, Mailliet F, Almeida OF, Jay TM, Sousa N. The prefrontal cortex as a key target of the maladaptive response to stress. J Neurosci. 2007;27(11):2781–7.
50. Ferro A, Carvalho AL, Teixeira-Castro A, Almeida C, Tome RJ, Cortes L et al. NEDD8: a new ataxin-3 interactor. Biochim Biophys Acta. 2007;1773(11):1619–27.
51. Gundersen HJ, Bendtsen TF, Korbo L, Marcussen N, Moller A, Nielsen K et al. Some new, simple and efficient stereological methods and their use in pathological research and diagnosis. APMIS. 1988;96(5):379–94.
52. West MJ, Slomianka L, Gundersen HJ. Unbiased stereological estimation of the total number of neurons in thesubdivisions of the rat hippocampus using the optical fractionator. Anat Rec. 1991;231(4):482–97.
53. Zar JH. Biostatistical Analysis, 4th edn. Prentice Hall, 1999.